Exp. Theo. NANOTECHNOLOGY 10 (2026) 1433-1447 https://doi.org/10.56053/10.3.1433

Airborne dust effect on soiling dynamics of inclined photovoltaic panels for low wind speed and no particle resuspension conditions

Rami M. Amro[1,*], *Saleh Salous*[2]

[1]Department of Applied Sciences, Palestine Technical University – Kadoorie, Aroub Branch, Hebron, Palestine
[2]Computer Science Department, Palestine Technical University – Kadoorie, Main Branch, Tulkarm, Palestine
*) Email: r.amro@ptuk.edu.ps

Received 11/2/2026, *Received in revised form* 18/4/2026, *Accepted* 19/4/2026, *Published* 15/7/2026

The performance of photovoltaic (PV) panels is strongly affected by dust accumulation, requiring a clear understanding of deposition mechanisms. Recent advances in nanotechnology and surface science are increasingly supporting mitigation strategies for this challenge. Under no particle bouncing conditions, and fixed simulation time, 10 sec., this study investigates the effects of panel inclination angle, low wind speeds ($\leq$ 2 m/s), and particle diameter on dust deposition behavior on PV surfaces. Results show that increasing the inclination angle raises the critical sliding velocity while reducing resistance to lift-off due to decreased normal loading. Particle size plays a dominant role in deposition dynamics, where larger particles $\geq$ 25 µm consistently deposit due to stronger gravitational and aerodynamic forces, while smaller particles exhibit a gradual size-dependent increase in deposition probability. Deposition distance and surface coverage increase with particle diameter, indicating stronger fouling by coarse particles. Mean deposition time decreases with increasing particle size and wind speed. Increasing wind speed enhances deposition rate and surface coverage, while having limited effect on the fraction of deposited particles under the no-bouncing assumption. The influence of inclination angle on deposition metrics is relatively weak under fixed particle size and wind conditions. Overall, deposition rate increases with particle size but decreases with increasing inclination angle, highlighting the importance of optimizing panel tilt to mitigate dust accumulation and improve PV performance.

Keywords: Photovoltaic Panel; Stochastic Brownian Motion; Dust Deposition; Dynamical System; Force Balance.

1. INTRODUCTION

The rapid worldwide expansion of photovoltaic (PV) installations has increased the need to better understand environmental factors that compromise long-term system efficiency and durability. Among the most critical of these factors is dust deposition, which has been widely recognized as a major contributor to performance degradation, especially in arid and semi-arid climates where airborne particles are abundant and rainfall-driven cleaning is infrequent [1–3]. Experimental and field-based studies consistently show that surface soiling can markedly reduce solar transmittance and power generation, with energy losses in harsh environments often surpassing 20–30% [2-4]. With PV systems increasingly deployed in desert and other high-solar-resource regions, accurate characterization of dust accumulation behavior is becoming increasingly important for improving system design, forecasting performance decline, and planning cost-effective cleaning and maintenance schedules.

Experimental analyses of dust sampled from operating PV systems have highlighted the highly complex physicochemical nature of deposited particles and their direct role in governing adhesion strength and optical losses. Investigations from Doha, Qatar, reported that the accumulated dust spans a wide particle-size spectrum, extending from submicron fractions to particles several tens of micrometers in diameter, while also exhibiting irregular shapes and mineral constituents primarily composed of silica, calcite, and clay-based materials [1]. This pronounced heterogeneity strongly influences surface roughness characteristics as well as the magnitude of particle–surface interaction forces. In addition, image-processing-based assessments have shown that dust deposition across PV surfaces is inherently non-uniform in space and continuously changes with time, with clear quantitative relationships observed between areal coverage fraction and electrical power reduction [3,5,6]. Collectively, these observations indicate that reliable soiling prediction frameworks must bridge microscale adhesion and particle mechanics with larger-scale atmospheric transport and deposition phenomena.

The accumulation of dust on tilted photovoltaic surfaces is controlled by a coupled interaction between gravitational settling, aerodynamic drag, lift effects, and electrostatic forces acting on suspended particles [7]. Force-balance models derived from classical Newtonian mechanics show that particle motion, impact behavior, and eventual deposition state are highly sensitive to key parameters such as particle diameter, local wind speed, and module inclination angle [7,8]. In the case of fine particulates under low Reynolds number flow conditions, viscous resistance becomes the dominant transport mechanism, suppressing inertial contributions and producing an overdamped response in which near-wall interactions largely dictate deposition behavior [7]. As particles enter the immediate vicinity of the PV surface, short-range adhesion mechanisms become decisive in determining whether they remain attached, rebound into the airflow, or migrate along the inclined substrate through sliding.

At the microscale, dust adhesion to PV glass is primarily governed by van der Waals, electrostatic, capillary, and contact deformation forces [9–13]. Classical Hamaker theory describes the dispersion interaction between spherical particles and flat substrates based on particle size and material properties [9,10], while contact mechanics models account for elastic deformation and surface energy effects [11,12]. Experimental studies show that van der Waals forces dominate under dry conditions, whereas capillary bridging becomes increasingly important at high humidity [13]. For micron-scale particles, these adhesion forces can far exceed gravity, which explains the strong persistence of fine dust on PV surfaces [13].

Electrostatic charging adds another important layer to dust adhesion behavior. In dry environments, particles can accumulate charge through triboelectric contact, atmospheric ionization, and corona-related processes [14–16]. This surface charge alters the overall interaction through Coulomb attraction and image-force effects, often strengthening adhesion beyond that predicted by van der Waals forces alone [14]. Experimental studies have shown that even modest charge levels can significantly increase the pull-off force of particles on dielectric glass surfaces [14]. Measurements using electrodynamic trapping also report broad charge distributions, commonly on the order of 10^5 - 10^6 elementary charges depending on particle size and composition [15]. These observations suggest that, under realistic desert conditions, electrostatic effects can become comparable to or even stronger than dispersion forces and therefore must be included in reliable predictive soiling models.

In addition to particle–surface adhesion, interparticle cohesion governs agglomeration and multilayer formation. Cohesive forces between dust particles can promote clustering, thereby modify effective aerodynamic diameter and alter deposition behavior [13], a similar mechanism can be achieved with the nanostructure coating [14]. Under humid conditions, capillary bridges significantly increase cohesion, enhancing resistance to detachment and wind-induced resuspension [13,15-18]. Such processes introduce nonlinear feedback mechanisms into dust accumulation dynamics, where deposited layers modify local flow fields and surface roughness, further influencing subsequent deposition.

Recent analytical models addressing the mechanics of dust on PV panels have attempted to integrate aerodynamic forces with adhesion criteria to predict detachment thresholds and equilibrium conditions [7]. These formulations typically resolve gravitational components parallel and normal to the panel surface, aerodynamic shear forces, and adhesive resistance. While these approaches provide valuable insights into the role of tilt angle and wind speed, they often assume simplified spherical particle geometry and neglect stochastic charge variability [7]. Furthermore, many models rely on deterministic adhesion parameters that do not fully capture experimentally observed heterogeneity in dust composition and surface roughness [1-3,6-13].

Parallel efforts in image processing and remote sensing have enabled non-invasive quantification of dust coverage on PV modules. Techniques including binarization, histogram analysis, statistical texture metrics, and color-matching algorithms have demonstrated reliable estimation of dust coverage with errors typically below 15% [3,6]. These methods provide essential validation data for modeling efforts but remain primarily empirical, lacking direct coupling with physical force models governing adhesion and deposition.

Despite substantial progress in experimental characterization, nanotechnology, and localized modeling, a comprehensive physics framework integrating aerodynamic transport, contact mechanics, electrostatic charging, and environmental variability remains limited. Existing studies often focus on isolated mechanisms - either adhesion force measurement [13], electrostatic effects [15,16], field dust characterization [1], or mechanical force balance formulations [7] - without fully coupling these domains into a unified predictive approach. This fragmentation restricts extrapolation to diverse climatic conditions and panel configurations in addition optimizing repellent coating nanostructure synthesis materials [14], for self-cleaning mechanisms of these solar cells.

The present study addresses this gap by developing a physically grounded modeling framework that integrates experimentally validated adhesion force laws, stochastic forces, and detailed mechanical force balance equations relevant to inclined PV panels. Using dust characterization data [1], adhesion measurements [13], electrostatic charging studies [15,16], and mechanical deposition models [7], the proposed approach aims to quantify deposition thresholds and stability conditions under realistic environmental parameters. Through this study, the work contributes new predictive capability toward understanding dust accumulation dynamics and provides a foundation for optimizing mitigation strategies and enhancing PV system reliability in dust-prone regions under low wind (few m/s) speeds and no bouncing conditions.

The study addresses the effect of wind speed, particle size, and inclination angle on dust accumulation levels. The article is arranged as follows: the next section shows the dynamical equations and forces included in the modelling. Model simulation and validation are explained in the section after. In section 4, we derive nearly closed form for the critical speeds needed for lift and sliding once the particle settle on the panel surface. In section 5, we change the particle diameter, inclination angle and wind speed and investigate its effect on the accumulation dynamics and the deposition time. Lastly, the conclusions section summary main results and recommendations.

2. MODEL EQUATIONS AND ASSUMPTIONS

The transport, deposition, and possible detachment of dust particles on an inclined photovoltaic (PV) panel are described using a Lagrangian framework in which each particle is tracked individually under the combined action of aerodynamic, body, stochastic, thermal, electrostatic, and surface-interaction forces. The particle motion is governed by Newton's second law,

$$m_p \frac{d\mathrm{v}_p}{dt} = \mathbf{F}_D + \mathbf{F}_G + \mathbf{F}_B + \mathbf{F}_L + \mathbf{F}_{Br} + \mathbf{F}_{Th} + \mathbf{F}_E + \mathbf{F}_{vdW} + \mathbf{F}_{cap} + \mathbf{F}_{fr}, \tag{1}$$

where v_p is particle velocity vector and $m_p = (\pi/6)\rho_p d_p^3$ is particle mass, with d_p and ρ_p denoting the particle diameter and particle density, respectively. The surrounding fluid velocity is denoted by v_f, and the relative velocity governing momentum exchange between the fluid and particle is defined as

$$\mathbf{u}_r = \mathbf{v}_f - \mathbf{v}_p. \tag{2}$$

The aerodynamic drag force is written as

$$\mathbf{F}_D = \frac{1}{2} C_D \rho_f A_p \parallel \mathbf{u}_r \parallel \mathbf{u}_r, \tag{3}$$

where C_D is drag coefficient, ρ_f is fluid density, and A_p is projected particle area. The drag coefficient of a rigid spherical particle is taken as a function of particle Reynolds number, $Re_p = \frac{\rho_f d_p ||u_r||}{\mu}$, where μ is dynamic viscosity. The piecewise drag law is adopted from [17].

$$C_D = \begin{cases} \frac{24}{Re_p}, & Re_p < 1 \\ \left(\frac{24}{Re_p}\right)\left(1 + 0.15\, Re_p^{0.687}\right), & 1 \le Re_p \le 800 \\ 0.44, & Re_p > 800 \end{cases} \tag{4}$$

By substituting A_p, we get the form;

$$\mathbf{F_D} = \left(\frac{\pi}{8}\right) \rho_f d_p^2 C_D \parallel \mathbf{u}_r \parallel \mathbf{u}_r \tag{5}$$

This formulation makes the drag force explicitly dependent on the instantaneous particle Reynolds number. Gravitational force is given by: $\mathrm{F}_G = m_p \mathrm{g}$, while the opposing buoyancy force is given by

$$\mathbf{F}_B = -\rho_f V_p \mathbf{g}, \qquad V_p = \frac{\pi}{6} d_p^3, \tag{6}$$

where V_p is particle volume and g is gravitational acceleration vector. To account for near-wall shear effects, a lift contribution is included as [18];

$$\mathbf{F_L} = \boldsymbol{\rho_f} * \boldsymbol{d_p^2} * \left||\boldsymbol{u_r}|\right|^2 * \boldsymbol{C_L}\, \boldsymbol{n_L} \tag{7}$$

where $\boldsymbol{C_L}$ is lift coefficient, $\boldsymbol{n_L}$ is unit normal vector to the wind velocity and particle velocity. Typical values for C_L are in the range 0.2 to 0.6 for low Reynolds numbers. For sufficiently small particles, stochastic molecular bombardment is represented through the Brownian force,

$$\mathbf{F}_{\boldsymbol{Br}} = \sqrt{\frac{\boldsymbol{2k_BT\gamma}}{\boldsymbol{\Delta t}}}\, \boldsymbol{\xi}, \qquad \boldsymbol{\gamma = 3\pi\mu d_p}, \tag{8}$$

where k_B is Boltzmann's constant, T is absolute temperature, Δt is numerical time step, γ is viscous damping coefficient, and ξ is a vector of independent Gaussian random variables with zero mean and unit variance.

Under non-isothermal operating conditions, thermophoretic migration is incorporated through [18]

$$\mathrm{F}_{th} = -6\pi\mu d_p \left(\frac{\frac{k_g}{k_p} + C_t Kn}{1 + 6C_m Kn}\right)\left(\frac{\mu}{\rho_f T}\right)\Delta T \,.\, \mathrm{n}\ \mathrm{n} \tag{9}$$

The thermophoretic force F_{th}represents the force acting on a dust particle due to a temperature gradient near the photovoltaic panel surface, driving the particle from hotter toward colder regions along the unit normal vector n. $k_g$and k_p are the thermal conductivities of the gas and particle material respectively, C_t and C_m are Talbot slip coefficients accounting for thermal and momentum accommodation effects, Kn is the Knudsen number. $\rho_a$is the air density, T is the absolute gas temperature, and ςT is the local temperature gradient magnitude, typically strongest normal to the heated PV surface. This force accounts for particle migration induced by spatial temperature gradients in the gas adjacent to the PV surface [19].

Electrostatic interactions are represented by [20], when the dust particle treated not as a point charge but with finite size, and also near the surface, we get the form

$$\boldsymbol{F_e = q_p E} + \left\{-\frac{\boldsymbol{q_p}^2}{\boldsymbol{16\pi\epsilon_0 z^2}} + \frac{\boldsymbol{q_p\, E\, d_p^3}}{\boldsymbol{16\, z^3}} - \frac{\boldsymbol{3\pi\epsilon_0 d_p^6 E^2}}{\boldsymbol{128\, z^4}}\right\} \mathbf{n}, \tag{10}$$

where q_p is particle charge, E is electric field assumed in the negative x-direction away from panel surface, ε_0 is vacuum permittivity, z is particle-surface separation distance, and n is unit normal directed outward from the PV surface. In this expression, the first term corresponds to the direct Coulomb force, whereas the second term represents the image-force correction associated with the interaction of a charged particle with a nearby dielectric or conducting surface [19].

As the particle approaches the PV surface, adhesive dispersion forces become increasingly important. The van der Waals interaction is modeled using the Hamaker sphere-plane formalism [9],

$$\boldsymbol{F_{vdW}} = -\left(\frac{\boldsymbol{A_H}}{6}\right)\left[\frac{\boldsymbol{d_p}}{2z^2} - \frac{\boldsymbol{d_p}}{(2z+\boldsymbol{d_p})^2} - \frac{2}{2z+\boldsymbol{d_p}} + \frac{1}{z}\right]\mathbf{n} \tag{11}$$

where A_H is Hamaker constant. This term captures the attractive intermolecular interaction between the dust particle and PV surface at short separation distances [9]. For distances $z \gg d_p$, F_{vdW} asymptotes to;

$$F_{vdW} \approx -\frac{A_H d_p}{8\, z^2}\ \mathrm{n} \tag{12}$$

while for very small distances, it approximates to;

$$\boldsymbol{F_{vdW}} \approx -\frac{\boldsymbol{A_H d_p}}{\boldsymbol{8\, z^2}}\ \mathbf{n} \tag{13}$$

Under humid ambient conditions, liquid bridges may form between the particle and the PV surface, producing an additional capillary adhesion force. This contribution is written as for very small separation between the spherical dust particle and the PV panel surface [21,22]

$$\mathbf{F}_{cap} = -2\pi d_p\, \gamma_w \cos\alpha\, \mathbf{n} \tag{14}$$

γ_w is surface tension of water, and α is the contact angle. This force represents the meniscus-induced attraction generated by the liquid bridge connecting the particle to the solid surface.

Once the particle contacts the panel, resistance to surface-parallel motion is described by a friction force,

$$\mathbf{F}_{fr} = -\,\mu_f F_N \frac{\mathbf{v}_t}{\|\mathbf{v}_t\|}, \tag{15}$$

where μ_f is coefficient of friction, F_N is normal contact load, and v_t is particle tangential velocity along the panel surface. For an inclined PV module tilted by an angle θ from the horizontal, the panel-based coordinate system is defined by the unit tangent vector

$$\mathbf{t} = (\cos\theta, 0, \sin\theta) \tag{16}$$

and the outward unit normal vector;

$$\mathbf{n} = (-\sin\theta, 0, \cos\theta). \tag{17}$$

The total force acting on the particle is then projected into tangential and normal components according to

$$F_{\mathrm{tot},\ \mathrm{t}} = \mathbf{F}_{tot} \cdot \mathbf{t}, \qquad F_{\mathrm{tot},\ \mathrm{n}} = \mathbf{F}_{tot} \cdot \mathbf{n}, \tag{18}$$

where F_{tot} denotes the resultant of all forces included in the model. Sliding is assumed to begin when the tangential driving force exceeds the frictional resistance, while lift-off or resuspension occurs when the resultant normal force becomes positive in the outward direction. This formulation provides a unified framework for predicting particle transport, deposition, sliding, and detachment on inclined PV panels under coupled aerodynamic, thermal, electrostatic, and adhesive effects.

3. MODEL SIMULATION AND VALIDATION

The above equation which includes all the terms for the possible forces are integrated using Euler-Maruyama method with time step ςt=10^{-4} sec, using the software Matlab-2015. All forces are used in the form they appear above. All parameters included in the simulation are shown in Table 1 below. The initial positions of the particles where set by to uniformly distributed, within the bounds of the PV panel, and starting near the lower edge of panel along x-axis. The panel assumed to have a length of 2.0 m and width 1.0 m. wind direction assumed to be facing the panel in the positive x-axis. The panel orientation is set to facing the negative x-axis and rising along the positive z-axis, with an inclination angle θ measured from the positive x-axis to the back of the panel. The deposition distance measured vertically to the surface of the panel. The runtime for the simulation is set to a fixed value (10 sec) to insure consistency between all measures. The temperature is set to 298 degrees Kelvin (K), and temperature gradient is set ΔT= -1000 K/m [23]. Moreover, to account for other fluid kicks we included the stochastic Brownian force, and modelled with a Gaussian white noise (see eq.8 above) with zero mean, and variance proportional to the temperature of the panel surface temperature. The electric field strength is chosen to 2X10^3 V/m assumed in the negative x-direction; a typical value reported in previous studies. The results of the model for the various considered forces are validated and compared against results published previously [9-13].

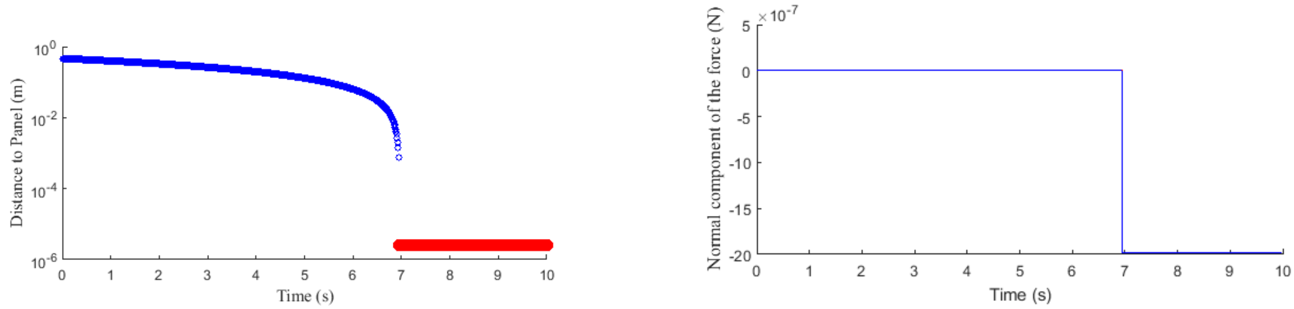

Figure 1 Distance to panel (left) and normal component of force on single particle tracked over period of 10 seconds. The blue line represents a normal distance of particle from panel before deposition, while the red line shows its distance from the panel after deposition.

To check further on the validity of the simulation, we tracked the particle distance – as shown in Figure 1 (left panel)- until the particle deposited on the plane. The initial normal distance of the particle from the plane is depicted by the distance value at t=0. As the code advance, the particle position and distance from the plane is dominated by the final sum of all the forces under consideration. From Figure 1 (right panel), we clearly see how the particle-panel distance is affected by the normal component of the force. We observe three phases for the motion: The first; while the particle far from the panel, it is affected by constant downward force component resulting in a quadratic decrease in it position relative to the panel.

This force is mainly due to the gravity force as observed from Figure 2. During this phase, the drag force is pushing the particle toward the panel. As a result, the particle nearing to the surface as the time pass. Other forces play a balancing role and contribute less but making the net normal component to be negative.

The second phase, is dominated by the sum of the rest forces which exceeds the drag force, and the particle continue in the sharp descending phase observed in Figure 1 (left panel). During this phase, as the particle nearing to the surface and about 50 µm, the capillary force kicks in. while the particle descending, we have noticed that drag force is about to change direction due to the rapid changes in the particle velocity. On the other hand, the electric force appears to play a significant role in this phase, as the its magnitude get larger. This phase is very short when compared to the first phase as forces are rapidly changing. The Brownian force (F_{Br} in legend of Figure 2) operates independently from the changes in the distance, and thus keeps doing the directional random kicks. But with existence of the larger forces, the path of the particle restricted toward the plane. The buoyant, and gravity forces maintain their constant value by definition.

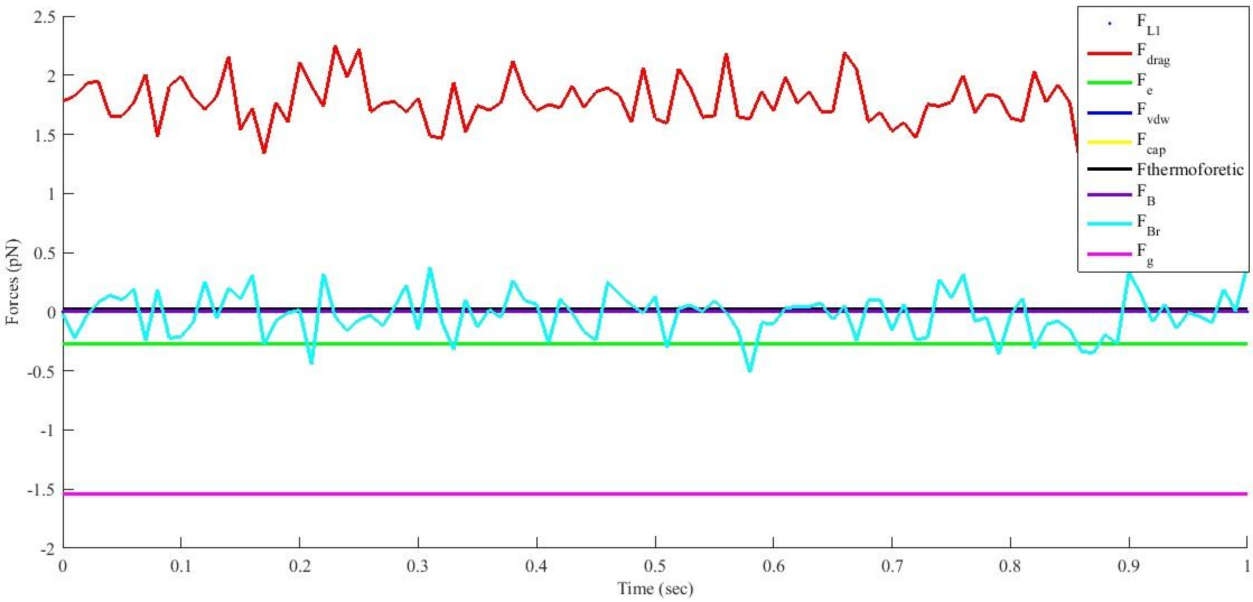

Figure 2 Panel normal component of different types of forces calculated. The particle assumed to have initial velocity equal to the wind speed (0 m/s). The legend shows the color for every force included.

The third phase, when the particle is near proximity (around 100 d_p in the simulation) the panel, at this scale, short range forces become the dominant, In particular the capillary and electric force. These force in addition to the drag force; all have large normal component and appear to dominate this phase. Van der Waals force, appear to have minimal effect as compared to this force, although it is a short-range force (in our simulation the particle position on the plane is not less than $\frac{d_p}{2}$), it appears to be not relevant for micro-sized spheres whose radius greater than few micrometers under humid conditions. Moreover, although the lift force is activated at this scale, Figure 3 shows it is about hundred orders of magnitude less than the drag force. Thus, the particle deposited eternally. The resuspension of the particle is not considered in this simulation. Lift and Brownian force may contribute to it.

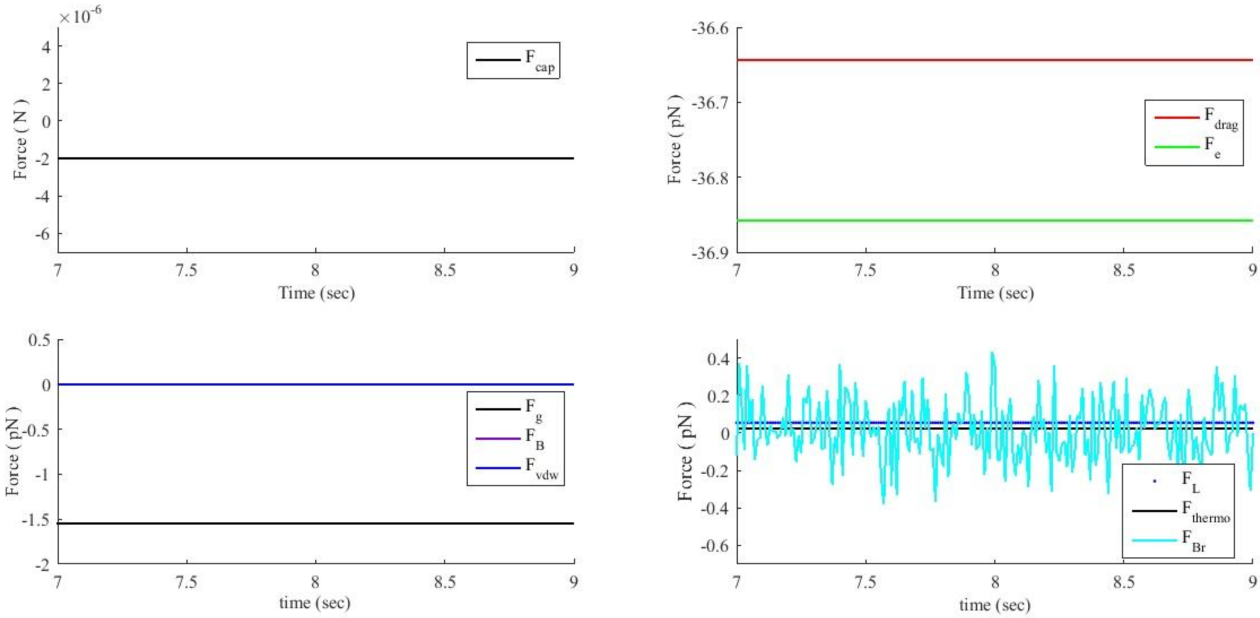

Figure 3 Acting forces during the deposition phase as a function of time, the legend from left to right and top to bottom respectively are: capillary, drag, electric, gravity, buoyant, van der Waals, lift, thermophoretic and Brownian force. Y-axis is the normal component of each force with respect to the surface of PV panel. All parameters are used from Table 1.

Now, we have validated the forces involved and shown the effect of every force and their dominant action during the three phases of the motion, we consider the following scenarios for different dust characteristics such as size, near the panel. It is well known that different regimes have different characteristics of the dust particles [24]. For example, they can be different in size, shape and chemical composition, we have treated them in general form and take widely used parameters specific for silica particle. The dust also varies according to the region and hence specific parameters used to represent their physical and chemical properties [1].

4. CRITICAL SLIDING AND LIFT SPEEDS

As the particle nearing to the surface, adhesion -Electric, capillary, and van der Waals - forces become more active and the particle is dominated to touch the surface, specifically for low wind speed in the z direction. To decipher the effect of the inclination angle, low wind speed and particle size on the particle settling on the panel after first time deposition.

Assuming that the electric field is in the negative direction, E= - E_0 $\boldsymbol{e_x}$, then we can write

$$F_E = -q_p\, E_0 e_x, \tag{19}$$

$$F_E \cdot t = -q_p E_0 cos\theta, \tag{20}$$

$$F_E \cdot n = q_p E_0 sin\theta \tag{21}$$

Using

$$F_E = -q_p E_0 cos\theta\, t + (q_p E_0 sin\theta + S_E(z))n \text{ , where } S_E(z) = -\frac{q_p^2}{16\pi\, \varepsilon_0 z^2} + \frac{q_p E_0 d_p^3}{16\, z^3} - 3\pi\frac{\varepsilon_0 d_p^6 {E_0}^2}{128\, z^4}$$

For the special case when the lift force is in the is pointing in the normal direction to the plane, i.e. , then $F_L = \rho_f * d_p^2 * \left||u_r|\right|^2 * C_L$ n, and the theromophoretic F_{th} can be approximated to zero, as ςT goes to zero near the surface. The drag force still reserves its 3D vector effect, and by assuming that the wind direction is a long the positive x-axis, $u_r = u_r\, e_x$

$$F_D = K_D(u_r . n\, n + u_r . t\, t) = K_D cos\theta\, u_r^2\, t - K_D sin\theta\, u_r^2\, n \qquad (22)$$

with $K_D = \left(\frac{\pi}{8}\right)\rho_f d_p^2 C_D$, The gravity and the buoyant force acting along the z direction, so they will have;

$W = (\rho_p - \rho_f)\left(\frac{\pi}{6}\right) d_p^3 g(-e_z) = -W\, sin\theta\, t - W\, cos\theta\, n$, where e_z is a unit vector pointing up

The van der Waals and capillary forces can be written as;

$F_{vdW} = -A_{vdw}(z)n$, $\quad F_{cap} = -A_c n$

Such that

$$A_{vdw}(z) = \left(\frac{A_H}{6}\right)\left[\frac{d_p}{2\, z^2} - \frac{d_p}{(2\, z + d_p)^2} - \frac{2}{2\, z + d_p} + \frac{1}{z}\right] \qquad (23)$$

$$A_c = 2\pi\, d_p \gamma_w cos\alpha \qquad (24)$$

Then the normal and tangential components of the net force acting on the particle can be written respectively as

$$F_t(u_r) = K_D cos\theta\, u_r^2 - W\, sin\theta - q_p E_0 cos\theta \qquad (25)$$

$$F_n(u_r, z) = \left(-K_D sin\theta + \rho_f d_p^2 C_L\right)u_r^2 + q_p E_0 sin\theta + S_E(z) - A_{vdw}(z) - A_c(z) - W\, cos\theta \qquad (26)$$

The critical speed needed to initiate particle motion in the tangential direction ($U_{slide,\, cr}$) can be calculated by enforcing the condition

$|F_t\,(u_r)| = \mu_f N(u_r, z)$, where (27)

We get the form for the critical wind speed for sliding, notice that for $F_n(u_r, z) > 0$, frictional force doesn't exist. Hence

$$F_t\,(u_r) = \mu_f F_n(u_r, z) \text{ for } F_n(u_r, z) < 0 \qquad (28)$$

$$U_{slide,cr}^2(z) = \frac{\mu_f[\; W\, sin\theta + q_p E^0 cos\theta + \left(W\, cos\theta + q_p E^0 sin\theta + S_E\,(z) - A_{vdw}(z) - A_c(z)\,\right)]}{[\,K_D cos\theta + \mu_f\left(-K_D sin\theta + \rho_f d_p^2 C_L\right)]} \qquad (29)$$

Or, equivalently,

$$U_{slide}, cr(z) = \left\{\, U_{slide,cr}^2(z)\right\}^{\frac{1}{2}} \qquad (30)$$

Now, we turn to calculate another important quantity, $U_{lift,cr}(z)$ which is the critical wind speed needed to lift the particle after settling on the surface. To do so, we force the condition $F_n(u_r, z) \geq 0$, which yield

$$U_{lift,cr}^2(z) = \frac{[\,A_{vdw}(z) + A_c(z) + W\, cos\theta - q_p E^0 sin\theta - S_E(z)]}{[-K_D sin\theta + \rho_f d_p^2 C_L]} \qquad (31)$$

$$U_{lift,cr}(z) = \left\{\, U_{lift,cr}^2(z)\right\}^{\frac{1}{2}} \qquad (32)$$

Figure 4 shows how the critical speed for different values of the inclination angle, we notice that, as the inclination angle increase, the critical sliding speed increases. This can be attributed that at higher inclination angles, the particle tends to slide down, and more drag need to prevent it from sliding, hence higher wind speeds is needed. On the other hand, increasing the angle decreasing the normal force, and thus lower wind lift speeds needed to lift off the particle from the surface. It is worth noting that the frictional force is being considered here. But in simulations, it is ignored as we don't study the dynamic state of the particle on the surface. The results in Figure 4 indicate that based on the inclination angle, the dust particle may slide or keep suspended on the panel. Thus, we can extract a critical angle for a specific wind speed and vice versa.

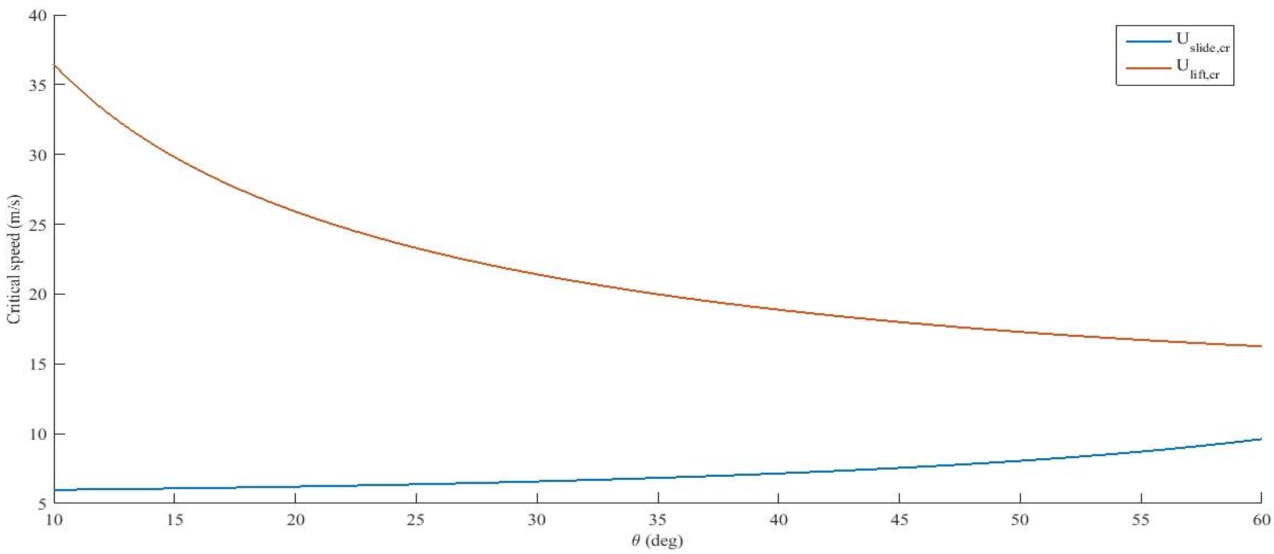

Figure 4 Critical sliding and lift speeds as a function of inclination angle. The parameters used to generate this figure are as in Table 1.

In general, Lower wind speeds are needed to lift the particle as while higher speeds are needed to drag the particle to the upper edge of the panel. On the other hand, preventing wind currents from reaching the panel, will result in the slippery motion of the particles to the lower edge to the PV. With these we have showed that critical wind speeds are optimal for changing soiling dynamics, hence affecting its performance. Albeit Other important factors to consider are solar radiation [25] and the thermal-electrical characteristics [26] of the modules.

5. EFFECT OF INCLINATION ANGLE AND PARTICLE DIAMETER ON THE PARTICLE DEPOSITION.

The inclination angle of the PV panel, plays an important role in the settling process of the suspended dust. To quantify this, we calculate the fraction of the deposited particles, and the relative covered area of the panel which is defined by the area of the deposited particles divided by the area of the panel, we assumed no interaction and no overlapping between the dust particles. Figure 5 (panels A and B), show that for low wind speeds (near 0.1 m/s) and particle diameter, as the inclination angle increases the fraction of the deposited particles increase, while for larger size particles all particles are deposited. This is attributed to the fact that in our simulation we stop tracking the particle dynamics, rather, we record its deposition position and allow the simulation to stop. While the fraction of the deposited particles reaching 100%, the fraction of the covered area keeps increasing for the obvious reason; larger particle covers larger deposition area.

Another two measures, which we found helpful in describing the results are, the mean deposition time

$$mean\ deposition\ time = \frac{sum\ of\ the\ time\ needed\ for\ every\ deposited\ particle}{number\ of\ the\ deposited\ particles} \quad (33)$$

And the mean deposition rate defined by

$$mean\ deposition\ rate = \frac{number\ of\ deposited\ particles}{mean\ deposition\ time} \quad (34)$$

The mean deposition time, show monotonic nonlinear decreasing trend as a function of the particle diameter (Fig.5-C), though its larger for large angles. which indicates that battling process between the acting forces. In particular the drag, the electric force, and the gravity is happening while the latter two

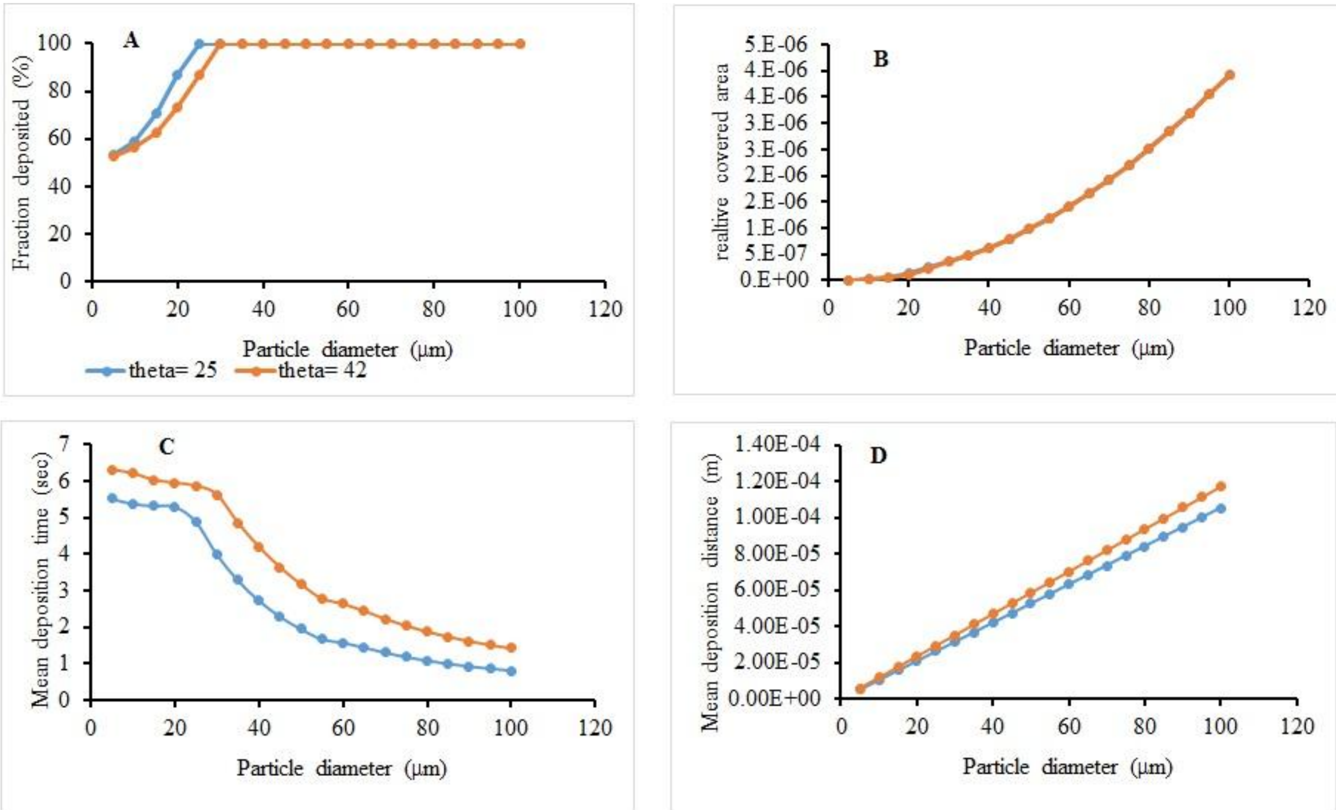

Figure 5 Effect of inclination angle and particle diameter on fraction of deposited particle (panel A), the relative covered area normalized to a total number of particles in simulation (panel B). Panel C represents the mean deposition time for deposited particles. Panel D, shows the mean deposition distance. The results are generated for relative humidity 60%, the wind speed is v=0.1 m/s and different angles shown in the legend of panel A. The rest of the parameters as stated in Table 1.

forces try to overcome the normal component of the drag force. Smaller particles have smaller gravity. The electrostatic force in our simulation assumed to be same for all particles whose diameter in the range of few tens of micrometers. Drag force is proportional to the cross-sectional area of the particle; it is small for smaller particles. Hence smaller particles take larger deposition time for the same inclination angle.

For larger inclination angle, the particle needs more time to reach same deposition place on the panel, as its z coordinate gets lower for larger inclination angle (θ=42°). Moreover, for larger particles, gravity and electrostatic force are teaming on comparable levels and pull the particle down, make it deposit faster and from further positions with respect to the panel. As shown in Figure 5-D, the distance from which the particle last move before hitting the surface - the deposition distance - increases with increasing the particle diameter and inclination angle. While its increase with increasing the diameter is explained in similar manner of the deposition time, its dependence on the inclination angle is explained by the increase in the normal component of the external electric field and gravity force; the majority of the other forces are along the normal direction with respect to the plane by definition.

For larger inclination angle, the particle needs more time to reach same deposition place on the panel, as its z coordinate gets lower for larger inclination angle (θ=42°). Moreover, for larger particles, gravity and electrostatic force are teaming on comparable levels and pull the particle down, make it deposit faster and from further positions with respect to the panel. As shown in Figure 5-D, the distance from which the particle last move before hitting the surface - the deposition distance - increases with increasing the particle diameter and inclination angle. While its increase with increasing the diameter is explained in similar manner of the deposition time, its dependence on the inclination angle is explained by the increase in the normal component of the external electric field and gravity force; the majority of the other forces are along the normal direction with respect to the plane by definition.

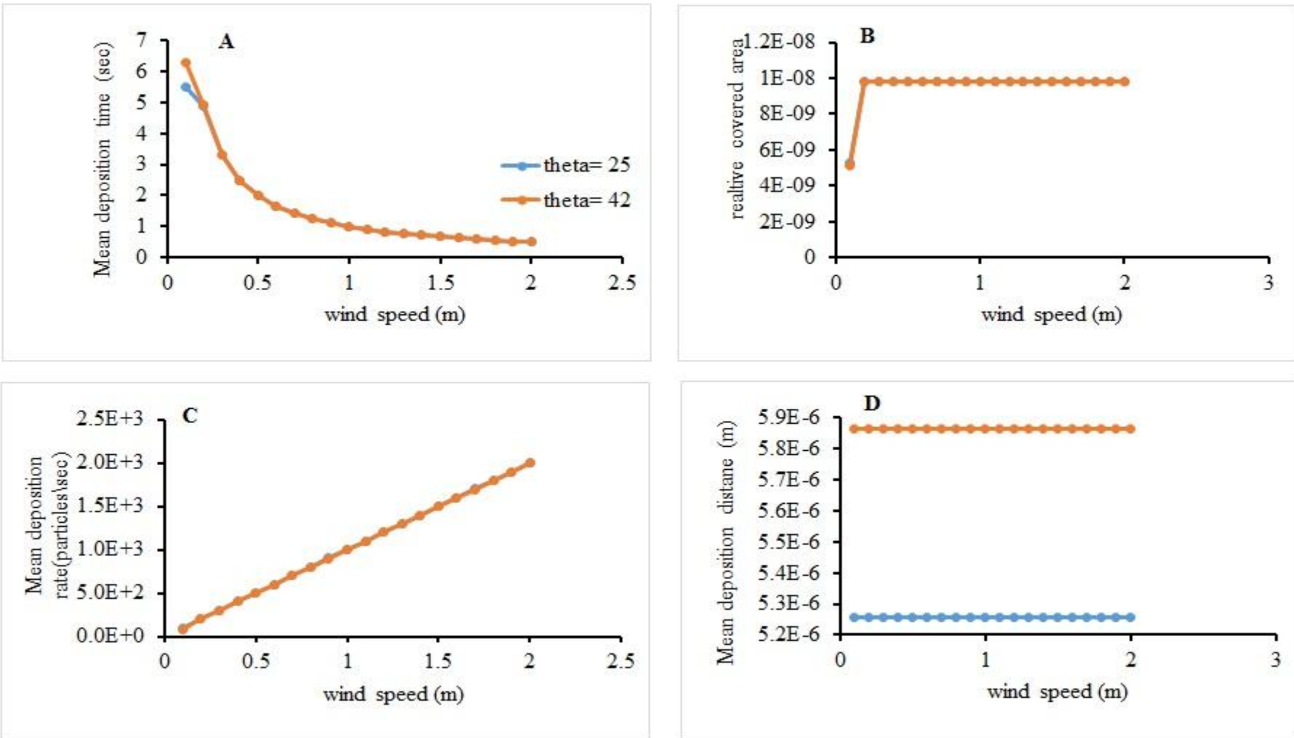

Figure 6 Effect of inclination angle and wind speed on the mean deposition time (A), relative covered area (B), mean deposition rate (C), and mean deposition distance (D). The results are generated for 60% relative humidity, particle diameter 5 μm and different angles shown in the legend of panel A. Other parameters are as shown in Table 1.

To check on further effects, the wind speed is varied between 0.1 to 2 m/s, and particle diameter is fixed to that of small dust particle d= 5 μm. Figure 6, shows the effect of wind speed on different quantitative measures for two different angles θ= 25° and 42°. In Panel A, we notice that the mean deposition time is decreasing monotonically as a function of the wind speed, indicating that large wind speeds cause more particle to deposit faster by moving in the positive x-direction closer to the panel, causing faster deposition. Figure 6-D shows that wind speed doesn't affect the mean deposition distance, indicating that the deposition is instantaneous and distance dependent when the particle in small distance from the panel. One would expect that for larger inclination angels, the mirror will be closer to the particle and deposit even faster, but this is not the case here for small particles. Figure 6 D, shows that this distance is barely affected by the inclination angle (see small numbers on the ordinate of Panel D); May be the angle-indifference for the small particles' deposition distance can be attributed to low wind speed, hence low drag force.   Never the less, Figure 5-D shows this is the case for large particles. Which we offered an explanation in the previous paragraph.

As a result of the no bouncing condition sought in this study, we notice that increasing the wind speed increases the deposition and covered fraction of the area (Figure 6 B and C), and this contradict the expectation from other studies where they included bouncing back events and resuspension conditions.

Table 1 List of parameters used in the simulation with definition, range of accepted values and reference from which the corresponding constant taken from.

Symbol	Definition	Accepted values / range in literature	Ref.
d_p	Dust particle diameter	5 µm (can vary 0.1–500 µm)	[27,28]
ρ_p	Particle density	2650 kg m^{-3}	[29]
ρ_f	Fluid density (dry air near 1 atm)	1.204 kg m^{-3}	[30]
µ	Dynamic viscosity of air	1.84e-5 Pa.s	[30]
g	Gravitational acceleration	9.80 $m\ s^{-2}$	
C_L	Lift coefficient	0.5	[31]
k_B	Boltzmann constant	1.380649×10^{-23} $J\ K^{-1}$	
C_s C_t , C_m	Related to thermophoretic coefficient	C_s = 1.17, C_t = 2.18, and $C_m \approx$ 1.14.	[19]
k_g	Gas thermal conductivity	≈ 0.0253–0.0263 $W\ m^{-1}K^{-1}$ for dry air at 20–25 °C.	[19]
k_p	Particle thermal conductivity	≈1.0–1.4 at room temperature.	[19]
q_p	Particle charge	0.5–2000 elementary charges used (-2000 X1.6X10^{-19} C)	[32]
E	Electric field strength	10^2 $V\ m^{-1}$ in calm weather and about 10^4 $V\ m^{-1}$in dust storms (used 2X10^2 $V\ m^{-1}$)	[33]
ε_0	Vacuum permittivity	8.85×10^{-12} $F\ m^{-1}$	
A_H	Hamaker constant	6.3×10^{-20} J	[13]
α	Contact angle	30° (20°–60° for clean to mildly contaminated glass /water	[34]
μ_f	Coefficient of friction	often modeled in the 0.12–0.13 range.	
γ_w	Surface tension of water	0.07274 at 20 °C and about 0.07197 at 25 °C.	[35]

This means, the detachment from the panel is attributed to the lift force and in a subsequent time the drag force, with both of these aerodynamic forces, the particle carried by wind and move away. We suggest not consider this to be a shortage of this study. Rather stress the fact that wind drive the dust to the panel, if the other holding down forces are strong enough, they hold the particle on surface, and if they are small on that scale, they would rather push it back to the wind stream causing changes in the magnitude and direction of its speed, and activating the lift force, with the help of Brownian kicks and bouncing of air molecules the particle resuspends to air and may go off the surface.

6. CONCLUSIONS

Dust accumulation on photovoltaic (PV) panels remains a major factor reducing their performance, making it an important to understand how particles deposit under different environmental conditions. This work examines dust deposition under no-bouncing conditions, focusing on the effects of panel inclination angle, low wind speeds (≤ 2 m/s), and particle size. Increasing the inclination angle was found to raise the critical sliding velocity while reducing resistance to particle lift-off due to lower normal forces. Particle size has a strong influence on deposition behavior, where larger particles (≥ 25 μm) tend to deposit more easily due to stronger gravitational and aerodynamic effects, while smaller particles show a gradual increase in deposition likelihood as size increases. Both deposition distance and surface coverage grow with particle diameter, indicating that coarse particles contribute more significantly to soiling. In contrast, the mean deposition time decreases as particle size and wind speed increase, reflecting faster transport toward the surface. Higher wind speeds enhance deposition rate and surface coverage, although the overall fraction of deposited particles remains largely unchanged under the no-bouncing assumption. The effect of inclination angle was comparatively weaker under fixed conditions of particle size and wind speed. Overall, the mean deposition rate increases with particle size but decreases markedly with increasing inclination angle, demonstrating that optimizing panel tilt was an effective strategy for mitigating dust accumulation and preserving PV performance.

Acknowledgements

The authors would like to thank the Palestine Technical University – Kadoorie for their financial support to conduct this research.

Conflicts of Interest

The authors declare that there is no conflict of interest regarding the publication of this manuscript.

References

[1] W. Javed, Y. Wubulikasimu, B. Figgis and B. Guo, Solar Energy, 142 (2017) 123 http://doi.org/10.1016/j.solener.2016.11.053
[2] T. Sarver, A. Al-Qaraghuli and L. L. Kazmerski, Renewable and Sustainable Energy Reviews, 22 (2013) 698 http://doi.org/10.1016/j.rser.2013.02.012
[3] W. K. Yap, R. Galet and K. C. Yeo, Renewable Energy, 80 (2015) 715 http://doi.org/10.1016/j.renene.2015.02.053
[4] E. F. Khanjer, B. Abul Al-Razak, M. S. Srayyih, M. A. Mohammed, A. A. Al-Sadooni, Experimental and Theoretical NANOTECHNOLOGY, 9 (2025) 385 https://doi.org/10.56053/9.S.385
[5] D.M. Atia, A.A. Hassan, H.T. El-Madany, A.Y. Eliwa and M.B. Zahran, Scientific Reports, 13 (2023) 13066 https://doi.org/10.1038/s41598-023-40168-8
[6] J. Abukhait, Ingénierie des Systèmes d'Information, 29 (2024) 533 https://doi.org/10.18280/isi.290214
[7] C. Xiong, Y. Zhang and X. Hui, Journal of Physics: Conference Series, 2356 (2022) 012006 http://doi.org/10.1088/1742-6596/2356/1/012006
[8] O. Bamisile, C. Acen, D. Cai, Q. Huang and I. Staffell, Renewable and Sustainable Energy Reviews, (2025). https://doi.org/10.1016/j.rser.2024.115073
[9] H. C. Hamaker, Physica, 4 (1937) 1058 http://doi.org/10.1016/S0031-8914(37)80203-7

[10] B. V. Derjaguin, Kolloid-Zeitschrift, 69 (1934) 155 http://doi.org/10.1007/BF01433225
[11] L. Zhang and C.Q. Ru, ASME Journal of Applied Mechanics, 86 (2019) 051004 https://doi.org/10.1115/1.4042574
[12] B. V. Derjaguin, V. M. Muller and Y. P. Toporov, Journal of Colloid and Interface Science, 53 (1975) 314 http://doi.org/10.1016/0021-9797(75)90018-1
[13] R. J. Isaifan, D. Johnson, L. Ackermann, B. Figgis and M. Ayoub, Solar Energy Materials and Solar Cells, 191 (2019) 413 http://doi.org/10.1016/j.solmat.2018.11.031
[14] A. Abdull Haleem and M. M. Abdullah, Experimental and Theoretical NANOTECHNOLOGY, 10 (2026) 93 https://doi.org/10.56053/10.1.93
[15] H. Kweon, S. Yiacoumi and C. Tsouris, Colloids and Surfaces A: Physicochemical and Engineering Aspects, 481 (2015) 583 http://doi.org/10.1016/j.colsurfa.2015.06.030
[16] L. V. Deputatova, V. S. Filinov, D. S. Lapitsky, V. Y. Pecherkin, R. A. Syrovatka, L. M. Vasilyak and V. I. Vladimirov, Journal of Physics: Conference Series, 653 (2015) 012129 http://doi.org/10.1088/1742-6596/653/1/012129
[17] F. Dioguardi, D. Mele and P. Dellino, Journal of Geophysical Research: Solid Earth, 123(2018) 144 https://doi.org/10.1002/2017JB014926
[18] P. Shi, R. Rzehak, D. Lucas and J. Magnaudet, Physical Review Fluids, 6 (2021) 104309 https://doi.org/10.1103/PhysRevFluids.6.104309
[19] L. Talbot, R. K. Cheng, R. W. Schefer and D. R. Willis, Journal of Fluid Mechanics, 101 (1980) 737 https://doi.org/10.1017/S0022112080001905
[20] A. Khachatourian, H.-K. Chan, A. J. Stace and E. Bichoutskaia, The Journal of Chemical Physics, 140 (2014) http://doi.org/10.1063/1.4862897
[21] G. Lian and J. Seville, Advances in Colloid and Interface Science, 227 (2016) 53 https://doi.org/10.1016/j.cis.2015.11.003
[22] A. Jaiswal, Langmuir, 39 (2023) 13178 https://doi.org/10.1021/acs.langmuir.3c01592
[23] S. Oh, B.W. Figgis & S. Rashkeev, Solar Energy, 211 (2020) 412 https://doi.org/10.1016/j.solener.2020.09.053
[24] V. Gupta, M. Sharma, M. R. K. and K.D Babu, Solar Energy 191 (2019) 596 https://doi.org/10.1016/j.solener.2019.08.079
[25] A. M. Hamed, A. A. Awad, A. M. Khalaf and O. T. Al-Taai, Experimental and Theoretical NANOTECHNOLOGY, 10 (2026) 141 https://doi.org/10.56053/10.1.141
[26] H. S. Faisal, C. M. Ahmed, A. A. Abeed, M. Q. Mohammed, A. T. Al-Douri, S. A. Ghanam, Z. T. Khattab, A. A. Ezat, M. A. M. Al-Doori, N. M. Ali, M. Ameri and M. M. Salih, Experimental and Theoretical NANOTECHNOLOGY, 9 (2025) 571 https://doi.org/10.56053/9.4.571
[27] A. Alraeesi, A. Shah and A. Hassan, Applied Sciences 13 (2023) 13162 https://doi.org/10.3390/app132413162
[28] Z. Quan, H. Lu, W. Zhao, C. Zheng, Z. Zhu, J. Qin, and M. Yue, Coatings 13 (2023) 49 https://doi.org/10.3390/coatings13010049
[29] P. Castellanos, P. Colarco, W. R. Espinosa, S. D. Guzewich, R. C. Levy, R. L. Miller, M. Chin, R. A. Kahn, O. Kemppinen, H. Moosmüller, E. P. Nowottnick, A. Rocha-Lima, M. D. Smith, J. E. Yorks and H. Yu, Remote Sensing of Environment, 303 (2024) 113982 http://doi.org/10.1016/j.rse.2023.113982
[30] K. Kadoya, N. Matsunaga and A. Nagashima, Journal of Physical and Chemical Reference Data, 14 (1985) 947 https://doi.org/10.1063/1.555744
[31] A. Dahham, I. Mohd Zainuri, M. A. A. Abdullah, A. A. Abdullah and M. F. Fauzan, Energies 16 (2023) 6397 https://doi.org/10.3390/en16176397
[32] G. Meng, D. Gao, S. Wang, Y. Xin and H. Zheng, Transactions of the Chinese Society of Agricultural Engineering, 30 (2014) 221 https://doi.org/10.3969/j.issn.1002-6819.2014.16.029

[33] S. A. Mallios, V. Daskalopoulou and V. Amiridis, Journal of Atmospheric and Solar-Terrestrial Physics 235 (2022) 105841 http://doi.org/10.1016/j.jaerosci.2022.106044
[34] T. Vukovic, J. Røstad, U. Farooq, O. Torsæter and N. van der Net, ACS Omega 8 (2023) 39837 https://doi.org/10.1021/acsomega.3c02448
[35] I. M. Hauner, A. Deblais, J. K. Beattie, H. Kellay and D. Bonn, The journal of physical chemistry letters, 8 (2017) 1599 https://doi.org/10.1021/acs.jpclett.7b00267